

Article

Comparative Study of Spark-Ignited and Pre-Chamber Hydrogen-Fueled Engine: A Computational Approach

Hammam Aljabri ^{1,*}, Mickael Silva ¹, Moez Ben Houidi ¹, Xinlei Liu ¹, Moaz Allehaibi ^{1,2}, Fahad Almatrafi ¹, Abdullah S. AlRamadan ³, Balaji Mohan ³, Emre Cenker ³ and Hong G. Im ¹

¹ Clean Combustion Research Center (CCRC), King Abdullah University of Science and Technology, Thuwal 23955, Saudi Arabia

² Mechanical Engineering Department, College of Engineering and Islamic Architecture, Umm Al-Qura University, Mecca 24382, Saudi Arabia

³ Transport Technologies Division, R&DC, Saudi Aramco, Dhahran 34466, Saudi Arabia

* Correspondence: hammam.aljabri@kaust.edu.sa

Abstract: Hydrogen is a promising future fuel to enable the transition of transportation sector toward carbon neutrality. The direct utilization of H₂ in internal combustion engines (ICEs) faces three major challenges: high NO_x emissions, severe pressure rise rates, and pre-ignition at mid to high loads. In this study, the potential of H₂ combustion in a truck-size engine operated in spark ignition (SI) and pre-chamber (PC) mode was investigated. To mitigate the high pressure rise rate with the SI configuration, the effects of three primary parameters on the engine combustion performance and NO_x emissions were evaluated, including the compression ratio (CR), the air–fuel ratio, and the spark timing. In the simulations, the severity of the pressure rise was evaluated based on the maximum pressure rise rate (MPRR). Lower compression ratios were assessed as a means to mitigate the auto-ignition while enabling a wider range of engine operation. The study showed that by lowering CR from 16.5:1 to 12.5:1, an indicated thermal efficiency of 47.5% can be achieved at 9.4 bar indicated mean effective pressure (IMEP) conditions. Aiming to restrain the auto-ignition while maintaining good efficiency, growth in λ was examined under different CRs. The simulated data suggested that higher CRs require a higher λ , and due to practical limitations of the boosting system, λ at 4.0 was set as the limit. At a fixed spark timing, using a CR of 13.5 combined with λ at 3.33 resulted in an indicated thermal efficiency of 48.6%. It was found that under such lean conditions, the exhaust losses were high. Thus, advancing the spark time was assessed as a possible solution. The results demonstrated the advantages of advancing the spark time where an indicated thermal efficiency exceeding 50% was achieved while maintaining a very low NO_x level. Finally, the optimized case in the SI mode was used to investigate the effect of using the PC. For the current design of the PC, the results indicated that even though the mixture is lean, the flame speed of H₂ is sufficiently high to burn the lean charge without using a PC. In addition, the PC design used in the current work induced a high MPRR inside the PC and MC, leading to an increased tendency to engine knock. The operation with PC also increased the heat transfer losses in the MC, leading to lower thermal efficiency compared to the SI mode. Consequently, the PC combustion mode needs further optimizations to be employed in hydrogen engine applications.

Keywords: hydrogen combustion; spark ignition; pre-chamber combustion



Citation: Aljabri, H.; Silva, M.; Houidi, M.B.; Liu, X.; Allehaibi, M.; Almatrafi, F.; AlRamadan, A.S.; Mohan, B.; Cenker, E.; Im, H.G. Comparative Study of Spark-Ignited and Pre-Chamber Hydrogen-Fueled Engine: A Computational Approach. *Energies* **2022**, *15*, 8951. <https://doi.org/10.3390/en15238951>

Academic Editors: Pedro Resende, Mohsen Ayoobi and Alexandre M. Afonso

Received: 18 October 2022

Accepted: 18 November 2022

Published: 26 November 2022

Publisher's Note: MDPI stays neutral with regard to jurisdictional claims in published maps and institutional affiliations.



Copyright: © 2022 by the authors. Licensee MDPI, Basel, Switzerland. This article is an open access article distributed under the terms and conditions of the Creative Commons Attribution (CC BY) license (<https://creativecommons.org/licenses/by/4.0/>).

1. Introduction

The transportation sector is one of the main contributors to greenhouse gas (GHG) emissions, which has promoted substantial research and development. The demand for passenger and cargo transport is increasing rapidly, while the net zero emission by 2050 scenario requires a 20% decrease in the transport sector emissions by 2030 [1]. As a result, research efforts are now focused on employing renewable fuels and more efficient

engines to reduce the carbon footprint. The hydrogen-powered internal combustion engine is gaining popularity due to its potential to achieve high brake thermal efficiencies of over 45% with emissions less than the EURO 6 standards without any after-treatment by utilizing lean ($\lambda > 2.5$) operation [2–11]. The high auto-ignition temperature and Research Octane Number ($\text{RON} \geq 130$) [12] of hydrogen compared to standard fuels make it a promising candidate fuel to mitigate the knocking tendency. However, its minimum ignition energy is lower than most hydrocarbon fuels, implying that hydrogen can be easily ignited by hot spots or residues in the combustion chamber. Studies with a pressure in the range of 0.2–1 atm and temperatures varying between 273–373 K have shown that the minimum ignition energy of hydrogen–air mixtures has an inverse relation with the square of pressure and with temperature [13]. If these trends are extrapolated to higher pressure and temperature, the minimum ignition energies of hydrogen–air mixtures will likely be significantly lower than reported for normal engine temperatures and pressures.

Having low minimum ignition energy may result in pre-ignition, which is defined as combustion during the compression stroke before the desired ignition timing. This may lead to a loss of control over combustion phasing, heavy knocking, and in extreme cases, mechanical failure of the engine. Although knock and pre-ignition have a nearly indistinguishable global impact, the causes of the two phenomena are vastly different [2]. Unlike knock, pre-ignition can be prevented with the proper engine design but knock mostly depends on the maximum compression ratio that can be used with a certain fuel [14]. Another difference is that knock can be mitigated by retarding the spark timing, while pre-ignition cannot be controlled in such a way.

The minimum ignition energy for hydrogen is highly sensitive to the air–fuel ratio as the stoichiometric condition ($\lambda = 1$) is approached from the lean side ($\lambda > 1$). This tendency is responsible for the experimentally observed fact that operating an H₂-ICE at or near the stoichiometric state in the absence of pre-ignition events is extremely challenging. As a result, for practical reasons, the minimum λ and peak power output can be restricted by the pre-ignition limit. The pre-ignition limit depends mainly on the engine specifications and operational conditions, of which consistent patterns have been discovered. For instance, it has been reported that the λ limit to prevent pre-ignition grows monotonically when the compression ratio (CR) [15–17] and mixture temperature are increased [16]. Moreover, the engine speed has also been demonstrated to influence [15,17], although the trend is more complicated owing to the associated effect of the residual mass fraction.

Hydrogen has a large flammability range of $0.14 \leq \lambda \leq 10$ at 1 atm and 298 K, compared to that of gasoline in the range of $0.25 \leq \lambda \leq 1.42$, implying that a hydrogen internal combustion engine will have more stable operation in a highly diluted environment, potentially leading to lower emissions and fuel consumption. One of the most researched modes of H₂-ICE is the port-fuel injection spark ignition (PFI SI) engine. Das [18] and White et al. [2] examined the performance and control techniques of this engine mode in depth, and reported that operating the engine under ultra-lean conditions ($\lambda \geq 2$) can reduce NO_x emissions to less than 100 ppm without the need for after-treatment. When operating at supercharged intake pressures of 2.6 bar, Nagalingam et al. [19] published data indicating values below 100 ppm for $\lambda > 2.5$. Natkin et al. [20] found 90 ppm emissions at $\lambda = 4$, which is similar. Ford's supercharged engine was operated at leaner conditions of $\lambda = 4.34$ to achieve emissions of 3–4 ppm [20]. The use of pure H₂ in SI engines have been extensively studied in literature [21–24]. Moreover, H₂ is also used to guarantee stable operation for different fuels such as, gasoline and compressed natural gas [25,26]. The H₂ addition lowers cycle-to-cycle variability and increases the lean-burn limit because of its low ignition energy and rapid flame speed. Thus, the use of pure H₂ permits high dilution rates, achieving very low NO_x emissions at lean and ultra-lean mixtures while keeping acceptable combustion stability.

The use of H₂ in a homogenous charge compression ignition (HCCI) mode was investigated thoroughly by [27] where high compression ratios ranging from 20:1 up to 45:1 under various air–fuel ratios was studied. It was found that with no charge preheating,

a very high compression ratio was required to reach the auto-ignition temperature of H₂. Under ultra-lean conditions ($\lambda \geq 2$), it was not possible to reach the auto-ignition temperature of H₂ using a CR < 26:1.

The use of an ultra-lean mixture is an effective strategy to further reduce emissions and improve fuel consumption. It has also been proven that lean mixtures will improve the indicated thermal efficiency by increasing the specific heat ratio, reducing heat transfer losses, and allowing for higher compression ratios to be used. Nonetheless, the ultra-lean mixture makes it challenging to ignite the charge, which could result in high incomplete combustion losses or misfires in more severe cases. In such a situation, pre-chamber combustion is considered a suitable solution to achieve stable combustion [28–30].

The pre-chamber (PC) consists of a spark plug that ignites the mixture in a small cavity, resulting in high temperature and pressure jets, which in turn travel through orifices to the main chamber leading to spatial ignition [31,32]. The flame propagation distance is shortened by the rapid penetration and dispersion of the hot turbulent jet. The main chamber (MC) combustion process is improved by the unburned intermediate products as well as the enhanced turbulence level resulting from the hot jet [33–36].

Depending on how the fuel is supplied, PCs are classified as active or passive. In the passive system, all the fuel is provided through the intake port into the MC, while in the active PC, an additional fuel injector provides a fraction of fuel into the PC to create local stratification [37–41]. Passive PCs have been used in gasoline engines in favor of simplicity, as a means to increase the combustion speed, reduce knocking tendency, and allow for higher compression ratios. However, one of the major limitations of the passive PC is that the lean burn limit cannot be significantly extended compared to conventional SI engines [38,42,43]. The active PC is thus considered to achieve the lean limit extension by the enrichment in the PC [44].

The objective of the present study was to identify the optimal operation modes to enable hydrogen-fueled engines by employing various lean-burn strategies. Starting with the SI engine mode as the baseline case, the effects of the overall air–fuel ratio, compression ratio, and spark timing on the auto-ignition tendency were numerically investigated in terms of combustion, thermal efficiency, and NO_x emissions. Subsequently, the use of pre-chamber under the same load conditions was assessed in comparison. Both active and passive PCs were used and investigated with different compression ratios, and their relative performance metrics were examined.

2. Numerical Setup and Model Validation

CONVERGE™ 3.0 [45] was used to conduct three-dimensional CFD simulations. For turbulence modeling, the original formulation of the RNG *k*– ϵ model was used [46]. The O'Rourke and Amsden [47] model was used to predict the heat transfer process. A real-fluid equation of state (Redlich-Kwong-Soave) combined with the gas species' critical properties consisting of pressure, temperature, and acentric factor for precise prediction of the Joule–Thomson effect with hydrogen [48] was used.

The SAGE detailed chemical kinetic solver with a detailed kinetic mechanism for H₂ combustion. Through the literature search, we adopted the mechanism developed by Park et al. [49], which was an optimized version of the original mechanism by Burke et al. [50] to improve the prediction at ultra-lean H₂ combustion conditions, in terms of ignition delay time and laminar flame speed validated against the experiment conducted by Bradley et al. [51].

Full-cycle simulations starting from the exhaust valve opening timing were conducted. The computational domain and mesh details are seen in Figure 1. A base grid of 4 mm was adopted, with both fixed embedding and adaptive mesh refinement (AMR) in the regions of interest, with the smallest grid size of 0.125 mm. In addition, three levels of dynamic refinement were used in the main chamber based on the gradients of velocity, temperature, and H₂ species mass fraction. Additional details on mesh and grid scaling can be found

in [52], including the detailed geometry of the PC that replaces the spark plug in the subsequent study. Considering the small volume, the interior of PC is sufficiently resolved.

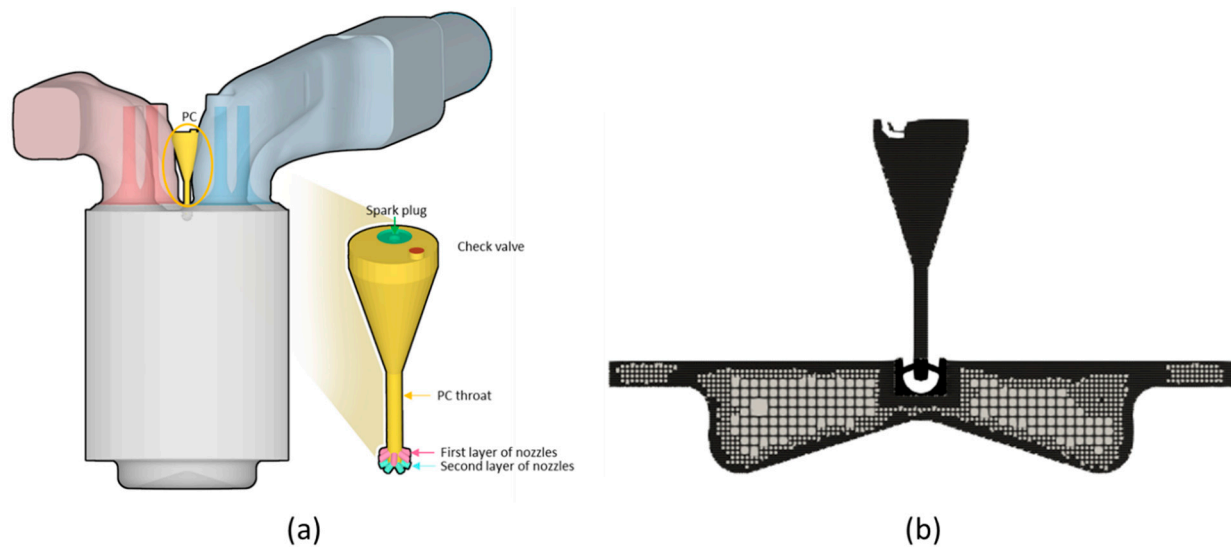


Figure 1. Schematic of: (a) computational geometry; and (b) grid control technique.

The engine specifications used in the simulations are listed in Table 1. The geometrical compression ratio corresponds to the standard bowl piston mounted on the Volvo D13C500 engines; details on engine setup and specifications are found in previous works [53]. This reference configuration was considered as we aimed to assess the utilization of hydrogen fuel in this engine with minimal modification of the geometry.

Table 1. Engine specifications.

| Engine Type | 4-Stroke |
|---|----------|
| Bore/stroke (mm) | 131/158 |
| Connecting rod length (mm) | 255 |
| Displacement volume (L) | 2.13 |
| Geometric compression ratio | 17:1 |
| Intake valve open ($^{\circ}$ aTDC) | 347 |
| Intake valve close ($^{\circ}$ aTDC) | −167 |
| Exhaust valve open ($^{\circ}$ aTDC) | −140 |
| Exhaust valve close ($^{\circ}$ aTDC) | 352 |
| H ₂ injected mass (mg/cycle) | 38.2 |

The fidelity of the current modeling approach was verified in previous studies using methane as a fuel with in-house data [54–56], which is briefly discussed in the current work. The selected cases refer to the equivalent experimental data with the maximum break torque. The initial and boundary conditions were further calibrated using 1D GT-Power; details on the methodology for calibration are shown in previous work [53]. The input parameters for the model have been experimentally measured, including the valve lift profiles, intake, exhaust, and pre-chamber fuel line pressure traces. For the pressure traces on both the pre-chamber and main chamber, the ensemble average of 500 experimental cycles is considered. The parameter Pre-chamber fueling ratio (PCFR) is the fraction of total fuel injected through the pre-chamber and more details can be found in Figure 2. The conditions for the validation are shown in Table 2. It should be mentioned that the simulated engine could withstand an in-cylinder peak pressure up to 220 bar.

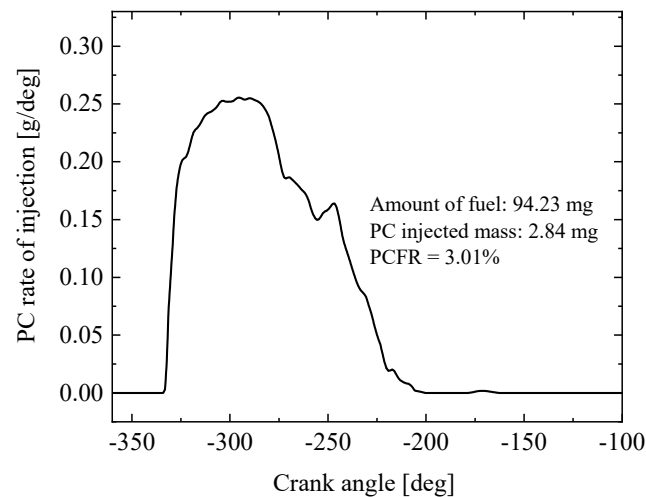


Figure 2. Pre-chamber fueling profile.

Table 2. Specifications of load and boundary conditions [57].

| | |
|--------------------------------------|------|
| Load (bar IMEP) | 9.5 |
| Engine speed (RPM) | 1200 |
| Effective compression ration | 11.1 |
| Intake pressure (bar) | 1.5 |
| Intake temperature (K) | 303 |
| Exhaust pressure (bar) | 1.7 |
| Exhaust temperature (K) | 800 |
| Total fuel mass (mg) | 94 |
| Global- λ | 1.8 |
| Pre-chamber fueling ratio (PCFR) (%) | 3 |
| Spark timing (CAD aTDC) | -13 |

The in-cylinder trapped fuel and total gas amounts are the key quantities to be matched between 3D CFD and 1D GT-Power solutions. For the 3D CFD, the field is initialized quiescently with the major species (CO_2 , CO , O_2 , N_2 , and H_2O), pressure, and temperature. Since the simulations ran for a full cycle starting at the exhaust valve opening, it allows for minimizing the field initialization before the combustion stroke. For the current simulations, the effective compression ratio was set to be 11.1, instead of the geometrical value of 11.5 in order to reproduce the experimental pressure trace. The PC fueling was performed during the intake stroke, as shown in Figure 2. Additional details on the injection strategy can be found in [53].

The validation of the pressure curve in Figure 3 showed satisfactory agreement between the experiment and the simulation. Further comparison of the engine performance parameters complemented the validation in Figure 3b. Small differences are inevitably caused by uncertainties in the employed physical and chemical models, but overall good prediction capability was demonstrated.

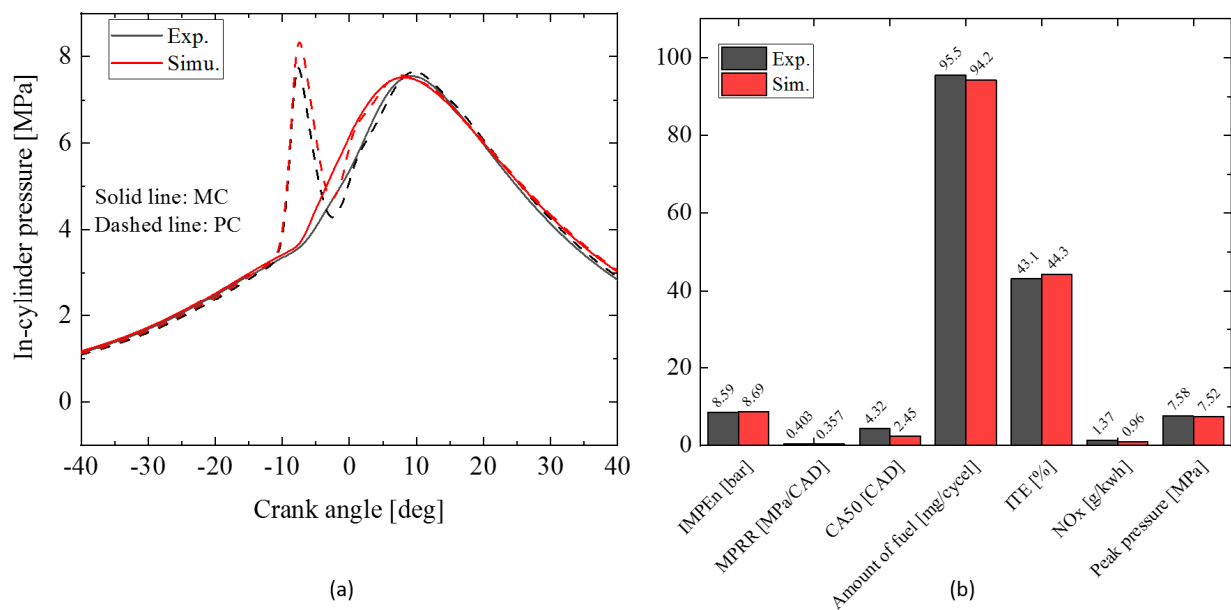


Figure 3. Validation of: (a) predicted pressure trace; and (b) predicted engine performance parameters for the reference case of Table 2.

3. Results and Discussion

The baseline case corresponded to a mid-load operation of a single-cylinder version of the Volvo D13C500 engine, which was extensively validated against experiments in previous studies [58,59]. The current investigation started with assessing the feasibility of converting this compression ignition (CI) diesel engine into operation with hydrogen in SI or PC modes. The practical goal was to implement a retrofit solution with minimal changes to an existing commercial engine architecture. The investigated controlling parameters included the compression ratio (CR), overall air–fuel ratio (λ), and spark timing (ST). In simulations, a maximum pressure rise rate (MPRR) of 1.5 MPa/deg, as suggested in [60], was used as the onset of abnormal combustion behavior. The calculated engine thermal efficiency, heat transfer loss, incomplete combustion loss, exhaust loss, and NO_x emissions, were collected and evaluated.

3.1. SI Combustion

The baseline case of H₂ spark ignition combustion is presented here as a reference case where the compression ratio was adjusted to 16.5:1 to account for the crevice volume which is not considered in the simulation as it would add unnecessary calculation cost and has negligible effect on the results. A lean mixture with $\lambda = 2.85$ was used to reduce the laminar flame speed and increase the minimum ignition energy to avoid auto-ignition and pre-ignition, respectively.

Figure 4 shows the pressure trace and heat release rate (HRR) of the baseline case where an abrupt pressure rise and HRR are observed. The MPRR, in this case, is 28.9 MPa/deg, which is considered too high for normal operation. This suggests that the mixture is highly reactive to yield nearly a HCCI mode of combustion. Based on the experimental work done by [27], it was not possible to reach the auto-ignition temperature of H₂ under lean conditions using a CR < 26:1 which raises some uncertainties about the chemical mechanism used in this study. The lack of the experimental data for H₂ combustion makes it a challenging task to validate this work. On the other hand, this study can provide general trends about the use of pure H₂ in CI diesel engines.

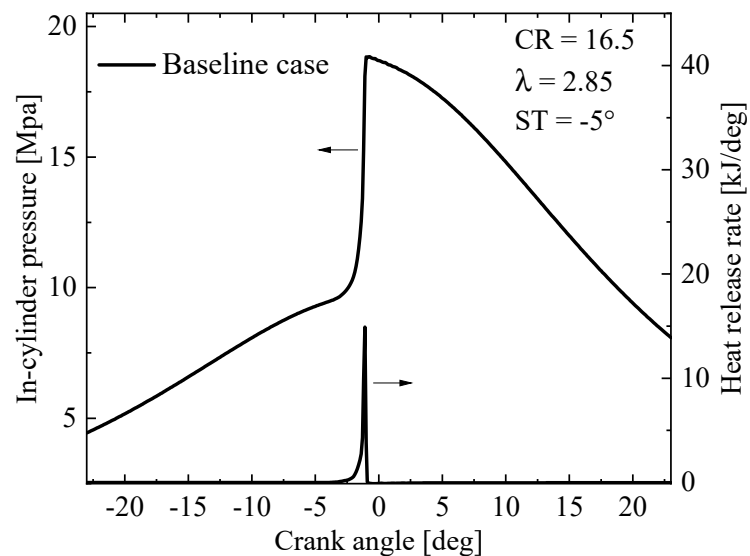


Figure 4. Predicted pressure and heat release rate traces for the baseline case.

Figure 5 shows the effect of using the spark plug as an ignition source. A slightly advanced combustion phasing is observed when the spark plug is used, while subsequent auto-ignition is evident from the steep MPRR in both cases (with and without spark ignition). This indicates that the spark plug assists in igniting the mixture leading to a spark-assisted compression ignition (SACI) combustion mode. Unlike in SI mode, knock in HCCI is mainly due to premature combustion in which ignition takes place before the desired time. It is challenging to control the ignition in such a combustion mode, which may limit the engine's operating range. It was observed that the HRR was slightly faster in the HCCI mode compared to the SACI mode.

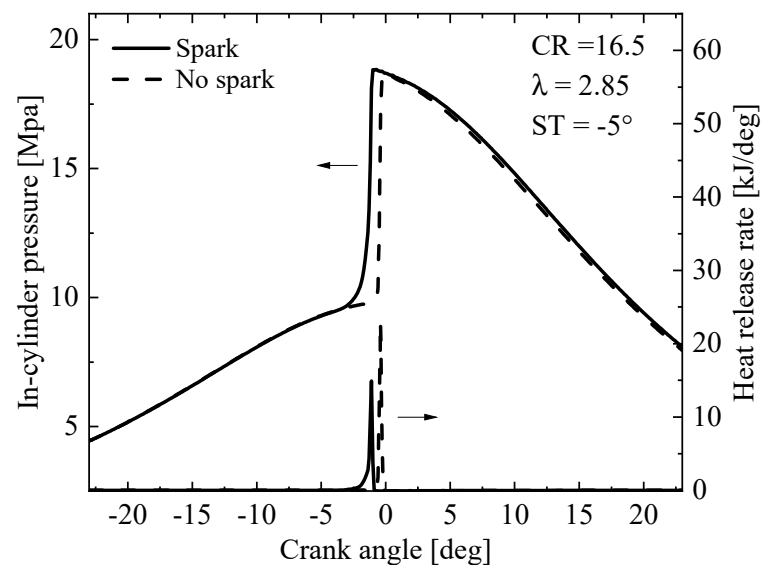


Figure 5. Effect of the spark plug on the predicted pressure and heat release rate traces for the baseline case.

Figure 6 shows the iso-surfaces of temperature at different times, where the occurrence of the auto-ignition is clearly seen. With SI, the auto-ignition was detected at 1.37 CAD bTDC (before the top dead center). As the flame propagated from the central position where the spark was located, a hot spot was observed near the cylinder walls. Without SI, the hot spot was observed at the same location at 1.47 CAD bTDC. It was thus concluded that in

the baseline case with a high CR, the combustion is primarily dominated by auto-ignition rather than flame propagation.

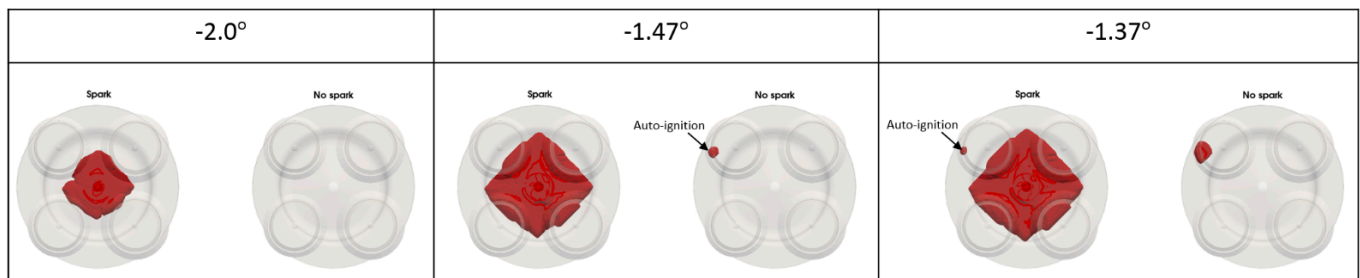


Figure 6. Comparison of temperature iso-surface (1600–3000 K) for spark vs. no-spark cases.

3.1.1. Effect of Compression Ratio

Engine CR is a critical factor directly affecting engine thermal efficiency and combustion. It is expected that the combustion duration decreases and the knocking tendency increases with an increased CR [61]. In the baseline case, a high MPRR was observed with an effective compression ratio of 16.5:1 even at very lean conditions ($\lambda = 2.85$). At high CRs, the compression temperature increased, which increased the reactivity of the fuel/oxidizer mixture. Thus, lowering the compression ratio may suppress the undesired auto-ignition/pre-ignition phenomena, making the combustion phasing easier to control with SI.

In this parametric study, at a fixed λ of 2.85, five CRs were selected ranging from 16.5 to 11.5 to investigate the effect on combustion performance and NO_x emissions. Figure 7 shows that as the CR is reduced, the combustion phasing becomes retarded, and the MPRR is mitigated. The heat transfer loss is also reduced due to the lower combustion temperature. Of these cases, a maximum indicated thermal efficiency (ITE) of 47.5% was obtained at the CR of 12.5.

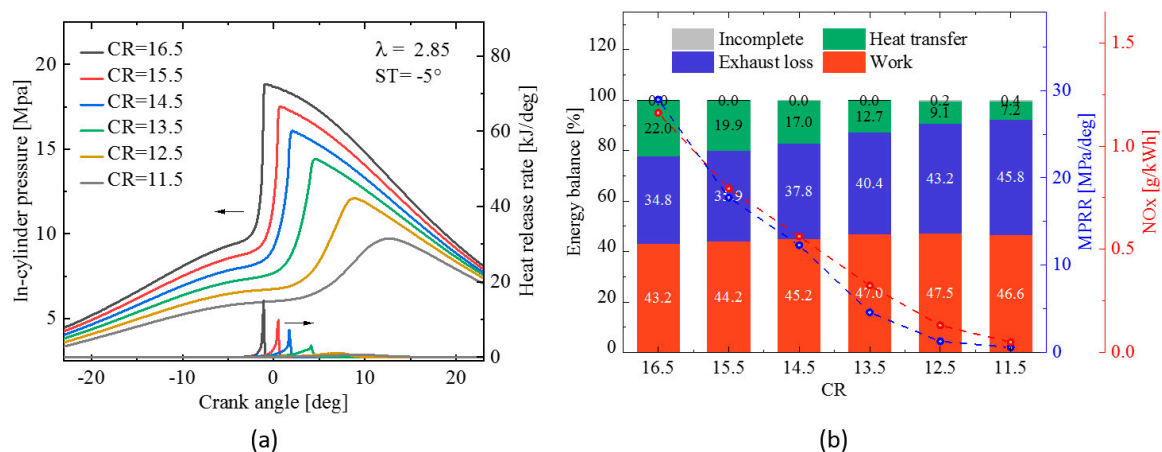


Figure 7. Comparison of: (a) pressure trace and heat release rate traces; and (b) efficiency for $\lambda = 2.85$ and $ST = -5$ CAD at different CRs.

Figure 8a shows the combustion duration, defined as the time interval between 5% (CA5) and 90% (CA90) of the total heat release, for different CRs at $\lambda = 2.85$. The results indicated that combustion duration is reduced almost linearly with an increased CR. As expected, the CR had a direct impact on the in-cylinder temperature, which explains the retarded combustion phasing and the lower NO_x emissions, as seen in Figure 8b. Note that the intake temperature and pressure remained constant as the CR was varied. With a CR below 12.5, the MPRR was kept under the threshold of 1.5 MPa/deg. For higher CRs, the

rapid combustion over a short period indicated an auto-ignition event, as demonstrated by the iso-surfaces of temperature illustrated in Figure 9.

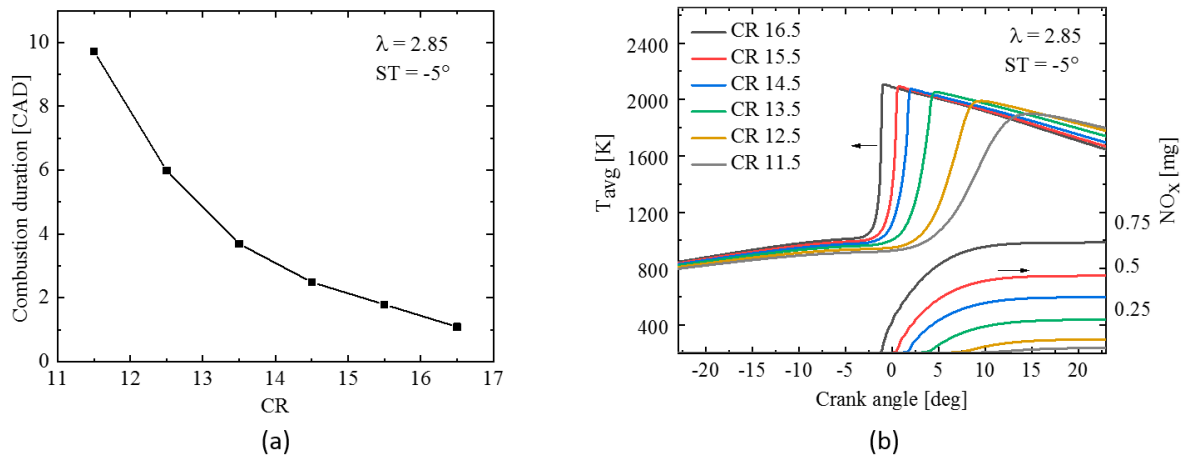


Figure 8. Comparison of: (a) combustion duration; and (b) in-cylinder average temperature for $\lambda = 2.85$ and $ST = -5$ CAD at different CRs.

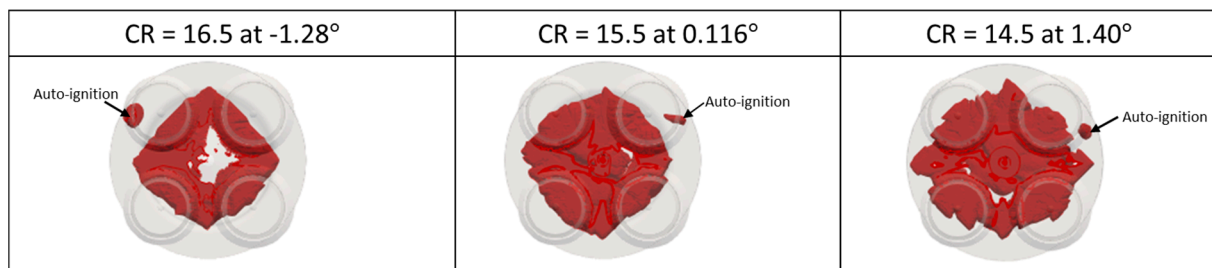


Figure 9. Comparison of iso-surface of temperature for $\lambda = 2.85$ and $ST = -5$ CAD at different CRs.

3.1.2. Effect of Air–Fuel Ratio (λ)

The effect of air–fuel ratio on auto-ignition was studied in this subsection. The previous case with a CR = 13.5 and $\lambda = 2.85$ was used as the baseline case. Two additional λ of 3.33 and 4 were also investigated. Note that the total injected fuel mass was kept constant by adjusting the intake pressure. For instance, the intake pressure was increased at a higher λ . It should be mentioned here that an intake pressure of 2.7 bar was used to reach a λ of 4. A further increment in λ would meet some challenges for practical limitations, such as a special boosting system, particularly at high engine loads.

The operation of the engine at leaner conditions would increase the minimum ignition energy, thus preventing pre-ignition events. In addition, it would mitigate the high reactivity of the hydrogen/air mixture resulting in lower laminar flame speed and longer auto-ignition delays. Moreover, the lean operation also leads to lowered adiabatic flame temperatures, reducing NO_x emissions and heat transfer losses. An almost zero NO_x level was achieved with leaner operation which was similarly reported by [62].

Figure 10 shows the pressure and HRRs traces at different λ with two CRs of 13.5 and 14.5. The results indicate that increasing λ beyond 2.85 effectively suppressed unexpected auto-ignition, as seen in Figure 10 (MPRR below 1.5 MPa/deg). However, increasing λ also resulted in a retarded combustion phasing and thus the higher incomplete combustion and exhaust losses. Of these cases, the case with a CR of 13.5 and $\lambda = 3.33$ achieved the highest ITE. The other cases suffered from misfire or auto-ignition issues. Therefore, further optimization by adjusting the spark timing should be performed to extend the high-performance operating range. The results obtained are consistent with what is reported by [63] where a CR = 10 and $\lambda > 2.5$ were used. The study showed that it was not feasible

to operate the engine with a $\lambda < 2.5$ due to the high-pressure rise rate, which is generated because of the ultra-fast flame speed.

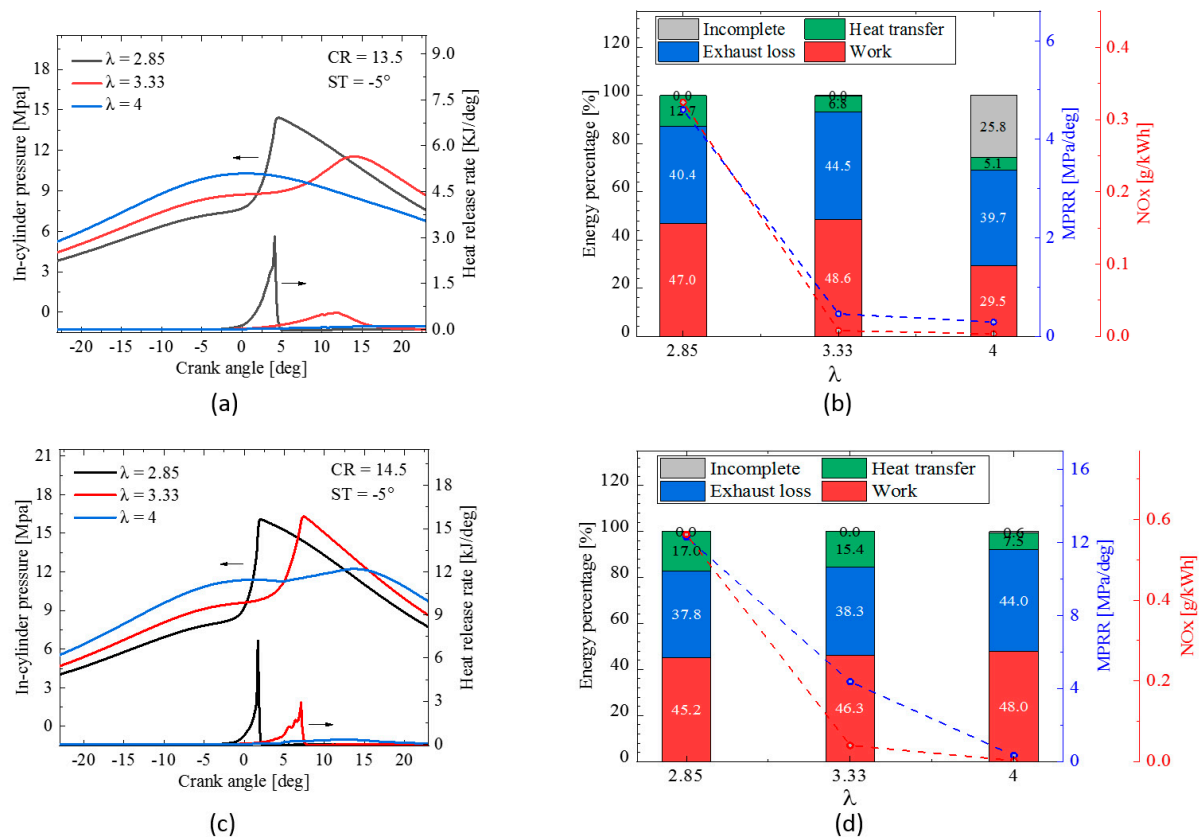


Figure 10. Comparison of: (a) pressure and heat release rate traces; (b) efficiency for CR = 13.5; (c) pressure trace and heat release rate; and (d) efficiency for CR = 14.5 using different λ at ST = -5° CAD.

3.1.3. Effect of Spark Timing

In this subsection, the effect of spark ignition timing was evaluated. The above cases with a CR of 13.5 and λ of 3.33 and 4 were used as the baseline cases. The spark timing (ST) sweep results are shown in Figures 11 and 12. By advancing the spark timing, the combustion and exhaust losses were reduced, while the heat transfer losses were increased due to the earlier combustion phasing. Within the limit of MPRR of 1.5 MPa/deg, the highest ITE of about 50% was obtained at a spark timing of 15 CAD bTDC with a CR of 13.5 and λ of 4.

In general, the advancement of the spark timing caused an increase in the MPRR due to near-TDC combustion heat release, which led to a shorter combustion duration. Comparing Figures 11 and 12 shows that it is preferable to go higher in CR as long as the mixture is lean enough to avoid auto-ignition. A higher achievable ITE was obtained at the higher CR (14.5) owing to the more isochoric combustion heat release near the TDC.

In addition, a high NO_x emission was generated when the spark time was advanced as the combustion temperature was increased. The overall level was always far below the Euro-6 limit (0.46 g/kWh). In some cases, advancing the spark time may lead to lower NO_x emissions, but considering that NO_x emission has the unit of g/kWh, the total absolute NO_x in kg was higher when the spark time was advanced.

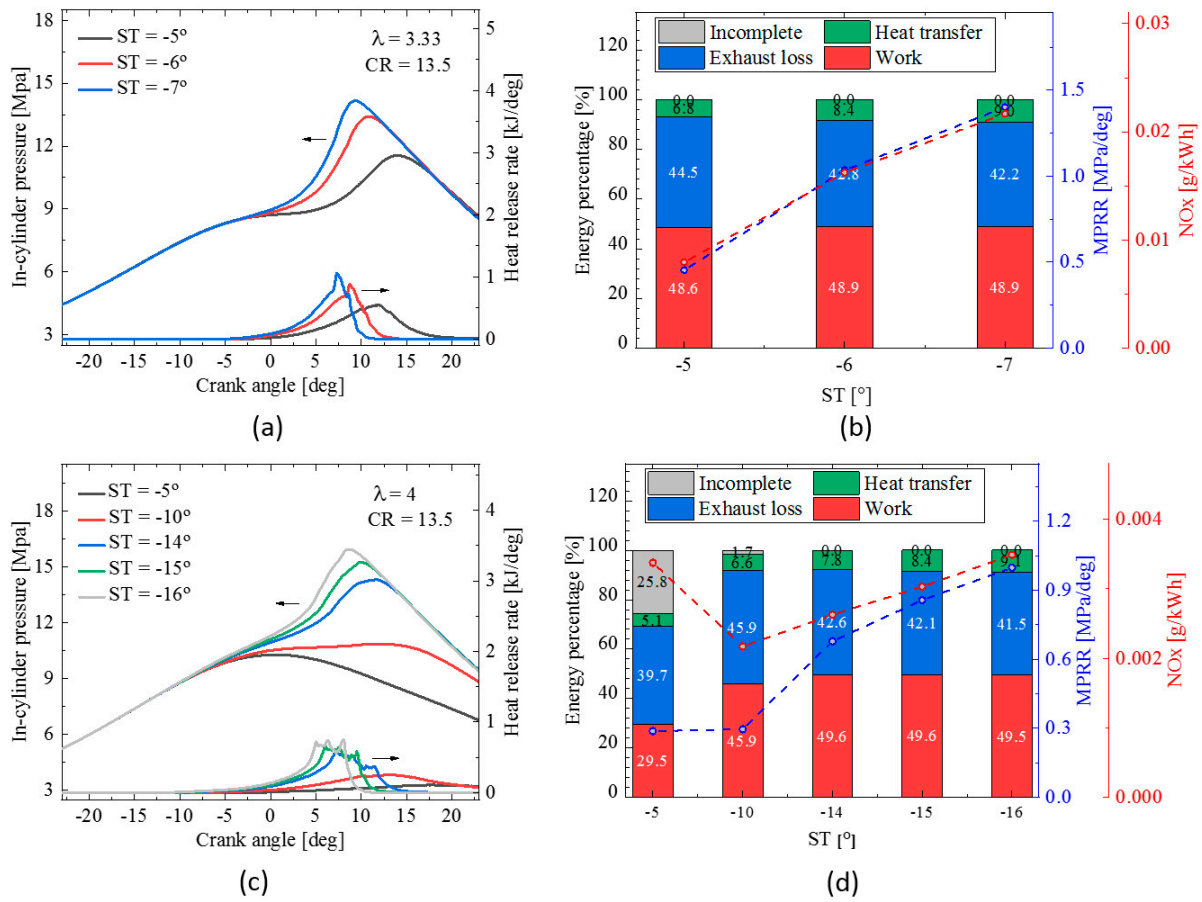


Figure 11. Comparison of: (a) pressure and heat release rate traces; (b) efficiency for and $\lambda = 3.33$; (c) pressure trace and heat release rate traces; and (d) efficiency for $\lambda = 4$ all set at CR=13.5 using different STs.

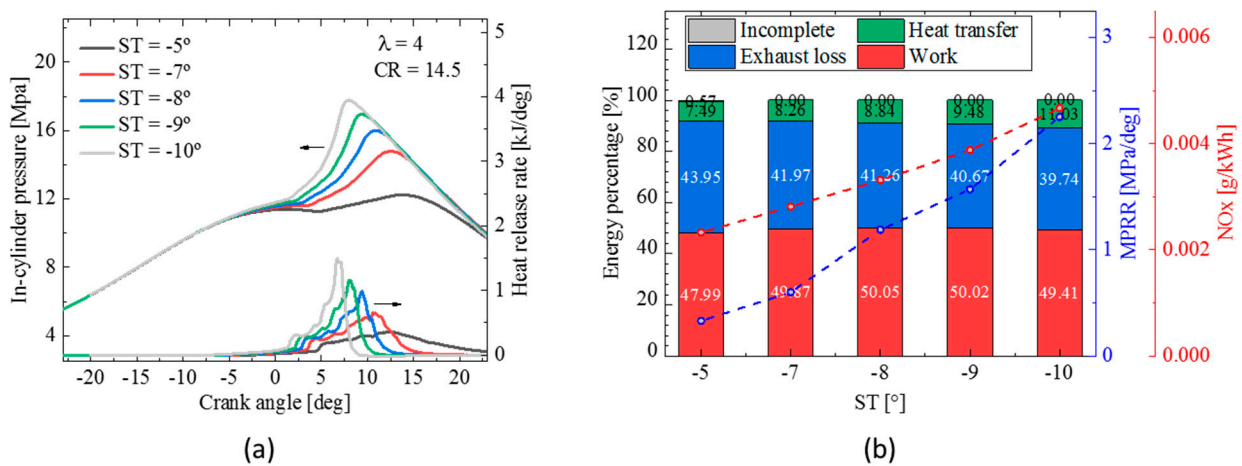


Figure 12. Comparison of: (a) pressure and heat release rate traces; and (b) efficiency for CR = 14.5 and $\lambda = 4$ using different STs.

The results obtained agree with [15] in terms of the optimized CR of 14.5 as they achieved a brake thermal efficiency of 38% for a 2 L four-cylinder engine. On the other hand, they used a $\lambda = 1.81$, while the optimized λ in this study was 4.

3.2. Pre-Chamber (PC) Combustion

The PC design was adopted based on the experiment done using methane as fuel [64]. The same engine configuration as in the SI mode was used, and the PC was mounted on the top of the cylinder head as indicated in Figure 1. Table 3 shows the PC specifications.

Table 3. PC specifications.

| PC Throat Diameter (mm) | 3.3 |
|-------------------------|-----|
| PC nozzle layer number | 2 |
| PC total nozzle number | 12 |
| PC nozzle diameter (mm) | 1.5 |
| PC nozzle angle (°) | 134 |

3.2.1. Passive PC

First, a passive PC was used where all the fuel was supplied through the intake port, which is defined as PCFR of 0%. A baseline case with $\lambda = 4$ and CR = 14.5 was adopted as an optimum case in which the high MPRR was suppressed, and the highest efficiency was achieved in the SI mode. Note that as the PC was installed, the total chamber volume was increased, but the squish height remained the same, causing a slight drop in the compression ratio by about 0.5.

The ST was adjusted to reduce the MPRR and optimize the combustion performance. Figure 13 shows the predicted pressure trace, HRR, and efficiency analysis for using a passive PC with different spark timing. As seen in Figure 13a, when the spark time is advanced, the predicted peak pressure and heat release rate are elevated as the combustion duration is shortened, which in turn results in a higher MPRR, as seen in Figure 14. On the other hand, advancing the ST generally results in higher ITE due to the more advanced combustion phasing. However, an excessively early ST results in the over-high heat transfer loss and, thus, a declining ITE. The simulations show that with the current PC setup, it is easy to trigger an extreme MPRR within the PC, even at a near-TDC ST like 4 CA bTDC. Therefore, other solutions like optimizing the PC geometries, control strategies, and lower CRs should be used.

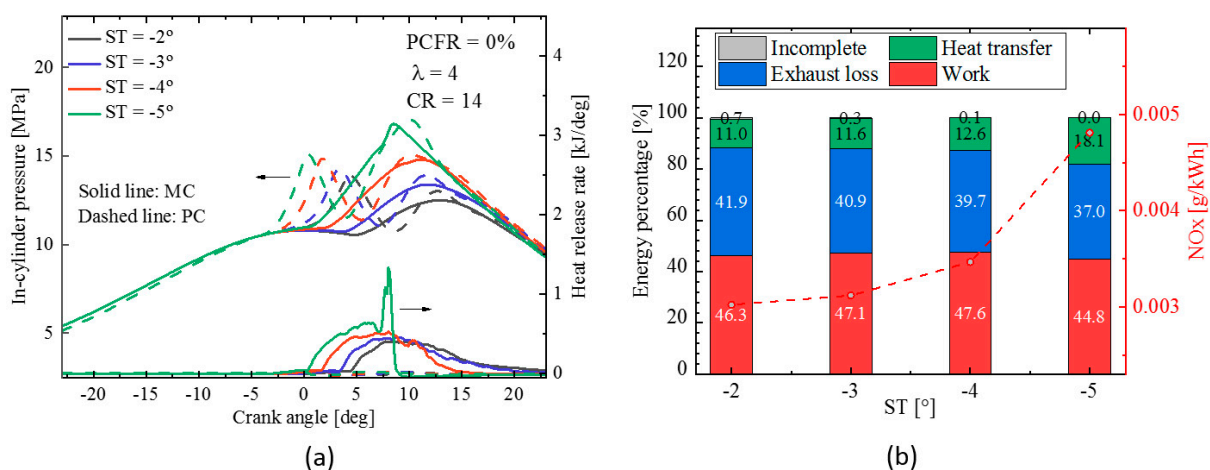


Figure 13. Predicted: (a) in-cylinder pressure and heat release rate traces; and (b) efficiency for PCFR = 0%, CR = 14, and $\lambda = 4$ using different STs.

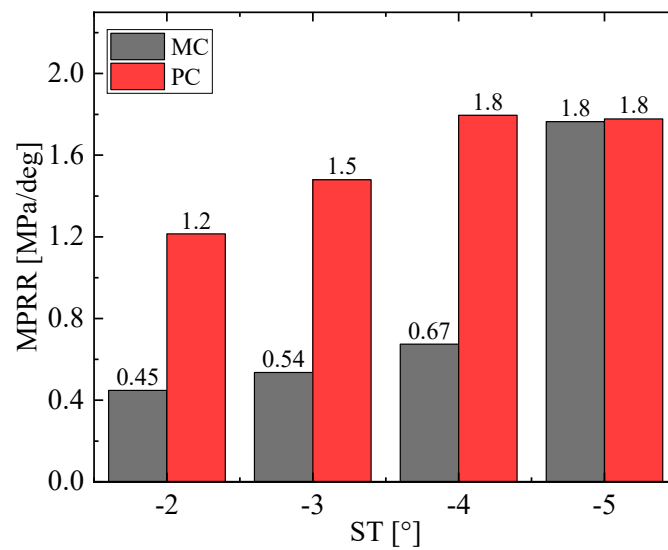


Figure 14. Predicted MPRR for PCFR = 0%, CR = 14, and $\lambda = 4$ using different STs.

As in the SI combustion mode, lowering the compression ratio from 14.5 to 13.5 can result in mitigating the high MPRR inside the PC and MC. Lowering the compression ratio also leads to lower combustion temperature and pressure, making both the MC and PC less prone to pre-ignition and knocking. As seen in Figure 15, at a lower compression ratio of 13, the ST needs to be advanced to increase efficiency. Note that as the ST is advanced, the combustion duration is shortened, resulting in faster and more abrupt combustion. This has a positive effect of lowering incomplete combustion losses. On the other hand, it has a negative effect of increasing heat transfer losses. It is also seen in Figure 15b that the reduction in the combustion losses resulted in an optimal ITE of about 47% at a ST of 5 CAD bTDC. Figure 16 shows the MPRR, and it indicates that the excessive pressure rise was significantly mitigated, as shown where the MPRR was still under the critical limit (1.5 MPa/deg).

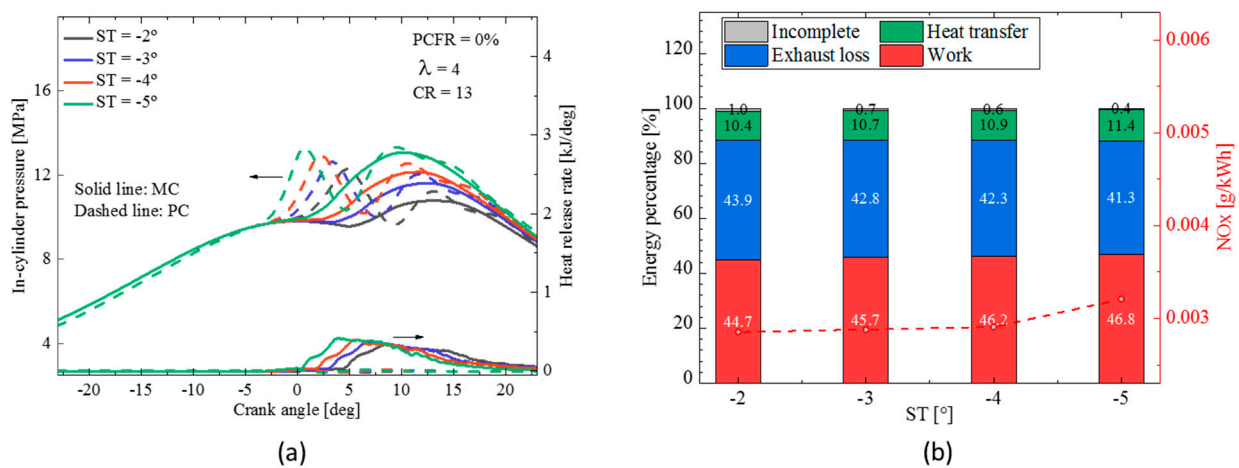


Figure 15. Predicted: (a) in-cylinder pressure and heat release rate traces; and (b) efficiency for PCFR = 0%, CR = 13, and $\lambda = 4$ using different STs.

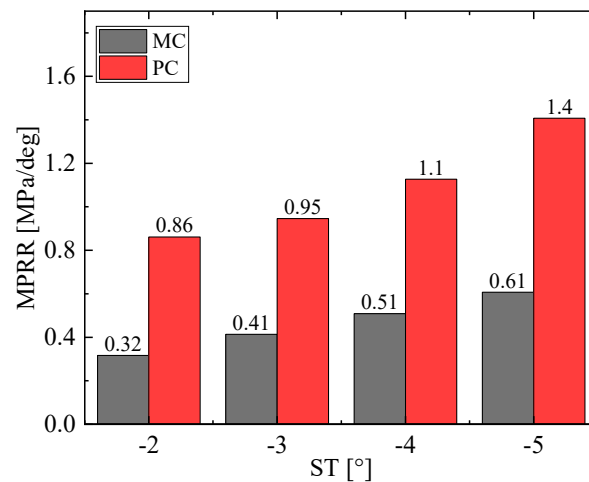


Figure 16. Predicted MPRR for PCFR = 0%, CR = 13, and $\lambda = 4$ using different STs.

3.2.2. Active PC

To assess the benefit of active PC, different values of PCFR were considered as the main parameter to control the combustion characteristics (including performance and emissions). The baseline case with a PCFR of 0% refers to a passive PC, while other PCFR values correspond to an active PC where a small percentage of the total fuel is provided through the PC while the majority is going through port injection. Figure 17 shows the predicted pressure and HRR traces with PCFR ranging from 0% up to 1.5% with an increment of 0.5%. As the PCFR is increased, so did the pressures in both MC and PC. Moreover, the combustion duration in the MC is also reduced, resulting in a more abrupt and higher heat release rate. However, the more advanced combustion phasing, and the resulting higher combustion temperature leads to a higher heat transfer loss and NOx emissions, as seen in Figure 17b. Due to the increased pressure difference between PC and MC, the faster and more intensely reacting jets are generated, as seen in Figure 18, which promotes the turbulent combustion within the MC and thus reduces the incomplete combustion loss, as indicated in Figure 17b. Nevertheless, as shown in Figure 19, the MPRR was overly high (>1.5 MPa/deg) with a non-zero PCFR.

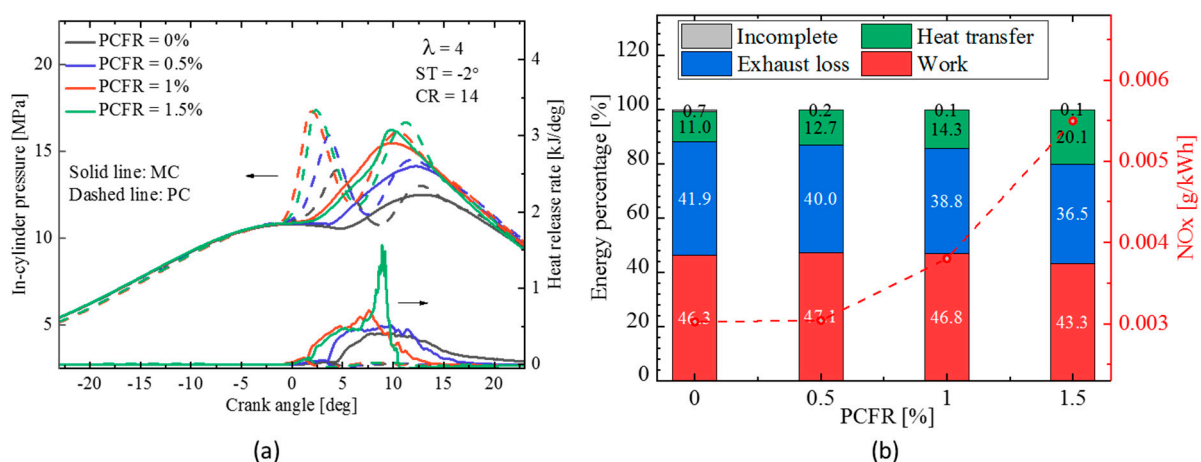


Figure 17. Predicted: (a) in-cylinder pressure and heat release rate traces; and (b) efficiency for CR = 14, and $\lambda = 4$, and $ST = -2^\circ$ using different PCFRs.

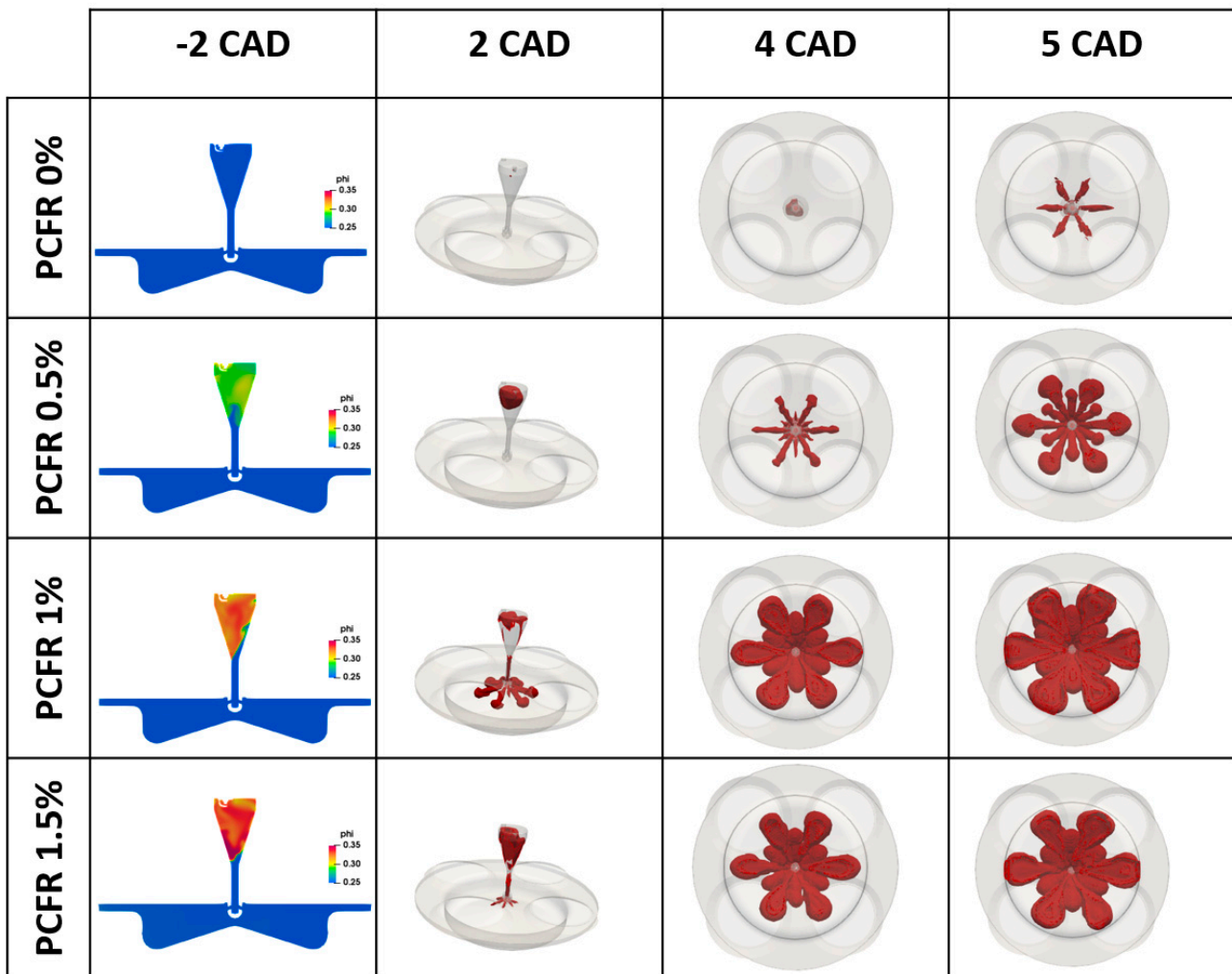


Figure 18. Comparison of ϕ and iso-surface (1600 K) of temperature using CR = 14, $\lambda = 4$, and $ST = -2^\circ$ using different PCFRs.

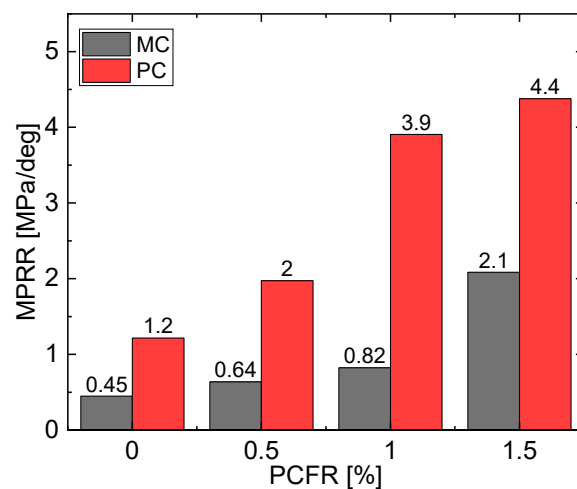


Figure 19. Predicted MPRR for $ST = -2$ CAD, CR = 14, and $\lambda = 4$ using different PCFRs.

3.3. Comparison between SI and PC Combustion Modes

A comparison between the SI and PC modes at similar operating conditions was summarized in this section. Figure 20 compares the pressure trace and HRR for $\lambda = 4$ in the

SI and PC modes. Compared to the SI mode, the PC mode resulted in a lower efficiency, which was mainly attributed to the significantly higher heat transfer losses. Figure 21 compares the rate of heat transfer for the optimized cases in the SI and PC. In both cases, the largest fraction of heat transfer losses was through the piston. In addition, the heat transfer losses through PC contributed to about 14.5% of the total heat transfer losses in the PC mode, while such a loss did not exist in the SI mode. As a result, the PC mode exhibited significantly higher heat transfer through the piston as the reactive turbulent jets from the PC enhanced the heat transfer rate through the piston, as seen in Figure 22. Despite the lower combustion temperature, the turbulent convection enhanced the heat transfer, yielding a higher total heat loss. The higher combustion temperature in the SI mode due to the higher CR does lead to higher NO_x emissions, although the NO_x emissions for both cases were low enough to raise practical concerns.

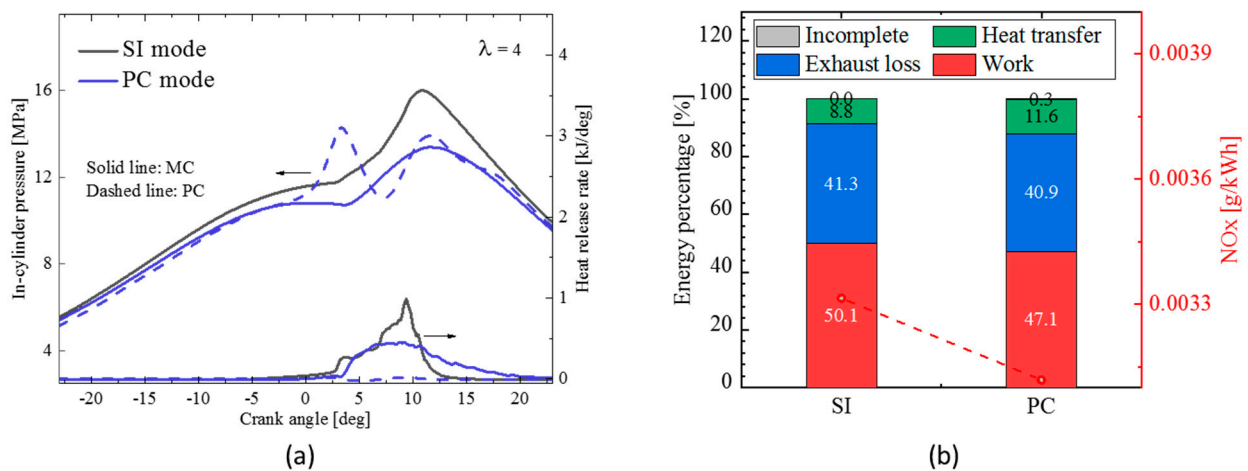


Figure 20. Predicted (a) in-cylinder pressure and heat release rate traces and (b) efficiency for SI mode (CR = 14.5 and ST = -8°) and passive PC mode (CR = 14 and ST = -3°) using $\lambda = 4$.

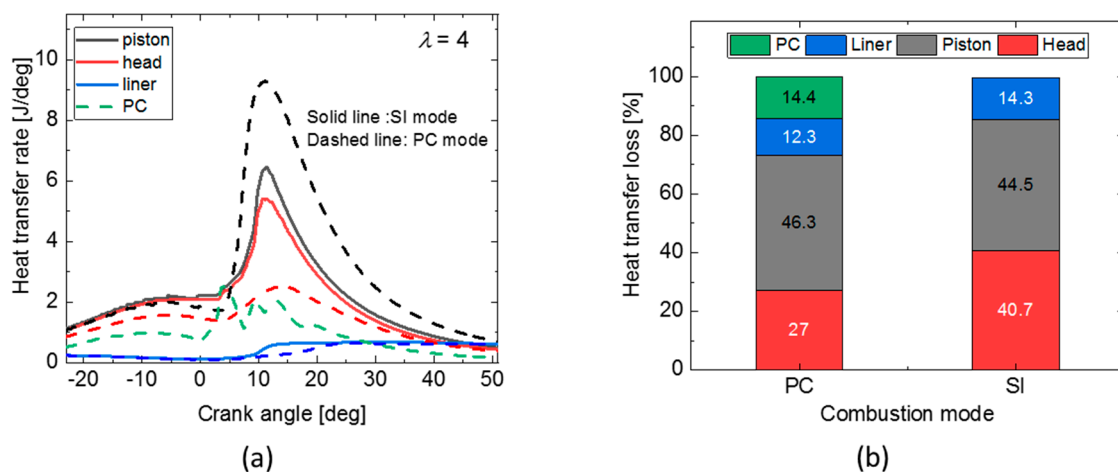


Figure 21. Comparison of the predicted: (a) heat transfer rates traces; and (b) % of heat transfer loss for SI mode (CR = 14.5 and ST = -8°) and passive PC mode (CR = 14 and ST = -3°) using $\lambda = 4$.

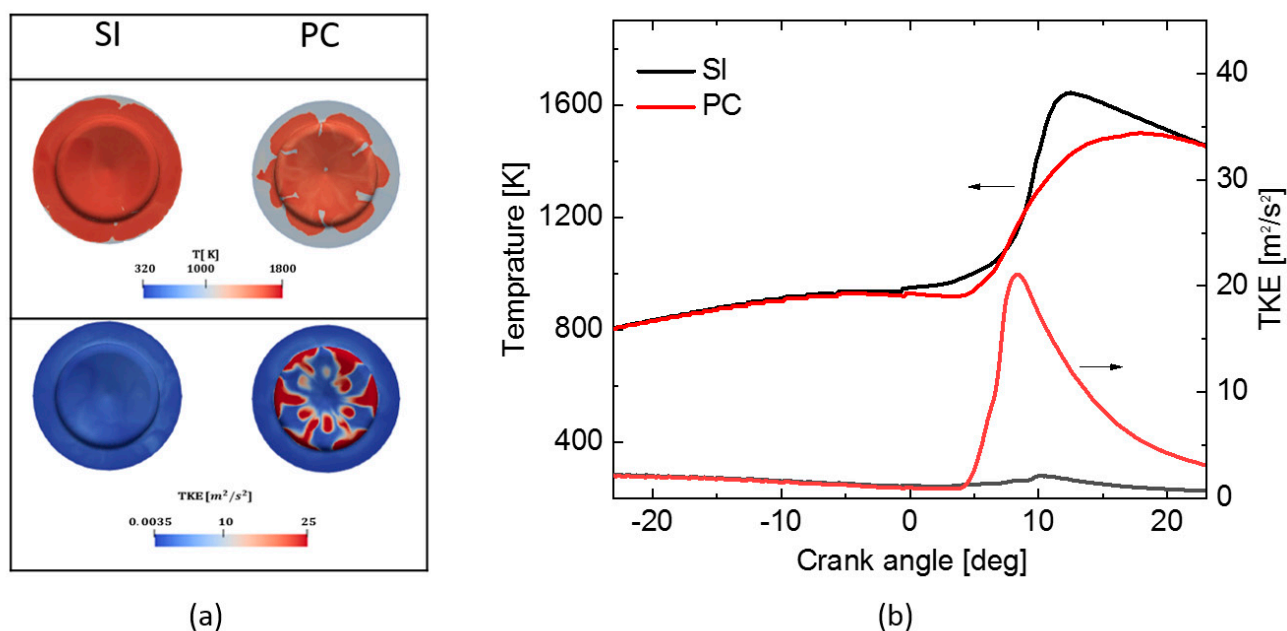


Figure 22. Comparison of the predicted piston (a) 3D distribution of temperature and TKE at 12 CAD, (b) near wall temperature and TKE for SI (CR = 14.5 and ST = -8°) and passive PC (CR = 14 and ST = -3°) modes using $\lambda = 4$.

4. Conclusions

In the current work, comprehensive CFD simulations of a heavy-duty engine converted to operate with pure H₂ under SI configuration were conducted. The effects of varying the air–fuel ratio, the compression ratio (CR), and the spark timing (ST) were investigated in order to identify the optimal range of operation at moderate load conditions. The results demonstrated that the optimal operation with SI mode would be at CRs of 13.5–14.5 and an air–fuel ratio of around 4. With such configurations, it was easier to adjust the ST to optimize the engine combustion performance by advancing the combustion phasing to improve the indicated efficiency while avoiding the abnormal auto-ignition that may cause high MPRR. The PC combustion mode was also investigated. The results indicated that the active PC would introduce higher MPRR and heat transfer losses inside both MC and PC compared to the passive PC. There was no additional means to optimize the passive PC at a high CR by adjusting ST due to the high MPRR. Thus, a reduction in CR combined with advanced ST was examined as a solution. In this case, the MPRR was within the normal range for engine operation, but the incomplete combustion losses increased.

As an overall comparison between SI and PC mode for the conditions under study, the PC mode generated a higher heat transfer loss owing to the significantly stronger jet flame–piston wall interaction and additional heat transfer through the PC assembly. Due to the high flame speed of H₂, even under ultra-lean conditions, a high ITE was achieved even at the SI mode by optimizing the ST and air–fuel mixture preparation. Moreover, combining moderate CRs with air dilution could be a potential solution to allow a larger range for engine controllability where PC can be more suitable compared to the normal SI mode. In the future, the numerical models used in this work will be validated against the experimental data under different loads.

Author Contributions: Conceptualization, H.A., M.S., M.B.H. and F.A.; Methodology, H.A.; Software, H.A.; Validation, H.A. and M.S.; Formal analysis, H.A.; Investigation, H.A., M.S., M.B.H., F.A., A.S.A. and B.M.; Resources, H.G.I.; Data curation, H.A.; Writing—original draft, H.A.; Writing—review & editing, M.S., M.B.H., X.L., M.A., F.A., A.S.A., B.M., E.C. and H.G.I.; Visualization, H.A., M.S., M.B.H. and F.A.; Supervision, M.B.H. and H.G.I.; Project administration, H.G.I.; Funding acquisition, A.S.A., B.M. and E.C. All authors have read and agreed to the published version of the manuscript.”

Funding: This research was funded by Saudi Aramco Research and Development Center FUELCOM3 program under Master Research Agreement Number 6600024505/01.

Acknowledgments: The paper is based on work sponsored by Saudi Aramco Research and Development Center FUELCOM3 program under Master Research Agreement Number 6600024505/01. FUELCOM (Fuel Combustion for Advanced Engines) is a collaborative research undertaking between Saudi Aramco and KAUST intended to address the fundamental aspects of hydrocarbon fuel combustion in engines, and develop fuel/engine design tools suitable for advanced combustion modes. The computational simulations utilized the Shaheen supercomputer at KAUST Supercomputing Laboratory. The authors thank Convergent Science Inc. for providing the CONVERGE license.

Conflicts of Interest: The authors declare no conflict of interest.

Abbreviation

| Abbreviation | Meaning |
|--------------|--|
| AMR | Adaptive mesh refinement |
| bTDC | Before top dead center |
| CA | Crank angle |
| CA5 | Crank angle of 5% cumulative heat release |
| CA90 | Crank angle of 90% cumulative heat release |
| CAD | Crank angle degree |
| CFD | Computational fluid dynamics |
| CI | Compression ignition |
| CO | Carbon monoxide |
| CR | Compression ratio |
| GHG | Greenhouse gas |
| HCCI | Homogenous charge compression ignition |
| HRR | Heat release rate |
| ICE | Internal combustion engine |
| IMEP | Indicated mean effective pressure |
| ITE | Indicated thermal efficiency |
| MC | Main chamber |
| MPRR | Maximum pressure rise rate |
| PC | Pre-chamber |
| PCFR | Pre-chamber fueling ratio |
| PFI | Port fuel injection |
| RNG | Renormalization group |
| RON | Research octane number |
| RPM | Revolution per minute |
| SACI | Spark assisted compression ignition |
| SI | Spark ignition |
| ST | Spark time |
| TDC | Top dead center |
| TKE | Turbulent kinetic energy |
| λ | Air–fuel ratio |

References

1. McBain, S.; Teter, J. Tracking Transport 2021; IEA: International Energy Agency. Available online: <https://policycommons.net/artifacts/1887399/tracking-transport-2021/2636759/> (accessed on 24 November 2022).
2. White, C.M.; Steeper, R.R.; Lutz, A.E. The hydrogen-fueled internal combustion engine: A technical review. *Int. J. Hydrog. Energy* **2006**, *31*, 1292–1305. [[CrossRef](#)]
3. Knop, V.; Benkenida, A.; Jay, S.; Colin, O. Modelling of combustion and nitrogen oxide formation in hydrogen-fuelled internal combustion engines within a 3D CFD code. *Int. J. Hydrog. Energy* **2008**, *33*, 5083–5097. [[CrossRef](#)]
4. Verhelst, S.; Maesschalck, P.; Rombaut, N.; Sierens, R. Increasing the power output of hydrogen internal combustion engines by means of supercharging and exhaust gas recirculation. *Int. J. Hydrog. Energy* **2009**, *34*, 4406–4412. [[CrossRef](#)]
5. Mohammadi, A.; Shioji, M.; Nakai, Y.; Ishikura, W.; Tabo, E. Performance and combustion characteristics of a direct injection SI hydrogen engine. *Int. J. Hydrog. Energy* **2007**, *32*, 296–304. [[CrossRef](#)]

6. Boretti, A.A.; Watson, H.C. Enhanced combustion by jet ignition in a turbocharged cryogenic port fuel injected hydrogen engine. *Int. J. Hydrog. Energy* **2009**, *34*, 2511–2516. [[CrossRef](#)]
7. Safari, H.; Jazayeri, S.A.; Ebrahimi, R. Potentials of NOX emission reduction methods in SI hydrogen engines: Simulation study. *Int. J. Hydrog. Energy* **2009**, *34*, 1015–1025. [[CrossRef](#)]
8. D’Errico, G.; Onorati, A.; Ellgas, S. 1D thermo-fluid dynamic modelling of an SI single-cylinder H₂ engine with cryogenic port injection. *Int. J. Hydrog. Energy* **2008**, *33*, 5829–5841. [[CrossRef](#)]
9. Kawahara, N.; Tomita, E. Visualization of auto-ignition and pressure wave during knocking in a hydrogen spark-ignition engine. *Int. J. Hydrog. Energy* **2009**, *34*, 3156–3163. [[CrossRef](#)]
10. Antunes, J.M.G.; Mikalsen, R.; Roskilly, A.P. An experimental study of a direct injection compression ignition hydrogen engine. *Int. J. Hydrog. Energy* **2009**, *34*, 6516–6522. [[CrossRef](#)]
11. Nieminen, J.; D’Souza, N.; Dincer, I. Comparative combustion characteristics of gasoline and hydrogen fuelled ICEs. *Int. J. Hydrog. Energy* **2010**, *35*, 5114–5123. [[CrossRef](#)]
12. Aleiferis, P.G.; Rosati, M.F. Controlled autoignition of hydrogen in a direct-injection optical engine. *Combust. Flame* **2012**, *159*, 2500–2515. [[CrossRef](#)]
13. Drell, I.L.; Belles, F.E. *Survey of Hydrogen Combustion Properties: Report 1383*; National Advisory Committee for Aeronautics: Cleveland, OH, USA, 1958.
14. Heywood, J.B. *Internal Combustion Engine Fundamentals*; McGraw-Hill Education: New York, NY, USA, 2018; ISBN 1260116107.
15. Tang, X.; Kabat, D.M.; Natkin, R.J.; Stockhausen, W.F.; Heffel, J. Ford P2000 hydrogen engine dynamometer development. *SAE Trans.* **2002**, *111*, 631–642.
16. Li, H.; Karim, G.A. Knock in spark ignition hydrogen engines. *Int. J. Hydrog. Energy* **2004**, *29*, 859–865. [[CrossRef](#)]
17. Al-Baghdadi, M.A.R.S. Effect of compression ratio, equivalence ratio and engine speed on the performance and emission characteristics of a spark ignition engine using hydrogen as a fuel. *Renew. Energy* **2004**, *29*, 2245–2260. [[CrossRef](#)]
18. Das, L.M. Hydrogen engines: A view of the past and a look into the future. *Int. J. Hydrog. Energy* **1990**, *15*, 425–443. [[CrossRef](#)]
19. Nagalingam, B.; Dubel, M.; Schmillen, K. *Performance of the Supercharged Spark Ignition Hydrogen Engine*; Indian Institute of Technology: Madras, India, 1983.
20. Natkin, R.J.; Tang, X.; Boyer, B.; Oltmans, B.; Denlinger, A.; Heffel, J.W. Hydrogen IC engine boosting performance and NOx study. *SAE Trans.* **2003**, *112*, 865–875.
21. Fischer, M.; Sterlepper, S.; Pischinger, S.; Seibel, J.; Kramer, U.; Lorenz, T. Operation principles for hydrogen spark ignited direct injection engines for passenger car applications. *Int. J. Hydrog. Energy* **2022**, *47*, 5638–5649. [[CrossRef](#)]
22. Oikawa, M.; Kojiya, Y.; Sato, R.; Goma, K.; Takagi, Y.; Mihara, Y. Effect of supercharging on improving thermal efficiency and modifying combustion characteristics in lean-burn direct-injection near-zero-emission hydrogen engines. *Int. J. Hydrog. Energy* **2022**, *47*, 1319–1327. [[CrossRef](#)]
23. Bao, L.; Sun, B.; Luo, Q. Experimental investigation of the achieving methods and the working characteristics of a near-zero NOx emission turbocharged direct-injection hydrogen engine. *Fuel* **2022**, *319*, 123746. [[CrossRef](#)]
24. Gürbüz, H.; Akçay, İ.H. Evaluating the effects of boosting intake-air pressure on the performance and environmental-economic indicators in a hydrogen-fueled SI engine. *Int. J. Hydrog. Energy* **2021**, *46*, 28801–28810. [[CrossRef](#)]
25. Niu, R.; Yu, X.; Du, Y.; Xie, H.; Wu, H.; Sun, Y. Effect of hydrogen proportion on lean burn performance of a dual fuel SI engine using hydrogen direct-injection. *Fuel* **2016**, *186*, 792–799. [[CrossRef](#)]
26. Molina, S.; Novella, R.; Gomez-Soriano, J.; Olcina-Girona, M. *Experimental Evaluation of Methane-Hydrogen Mixtures for Enabling Stable Lean Combustion in Spark-Ignition Engines for Automotive Applications*; No. 2022-01-0471. SAE Technical Paper; SAE: Warrendale, PA, USA, 2022.
27. Lee, K.J.; Kim, Y.R.; Byun, C.H.; Lee, J.T. Feasibility of compression ignition for hydrogen fueled engine with neat hydrogen-air pre-mixture by using high compression. *Int. J. Hydrog. Energy* **2013**, *38*, 255–264. [[CrossRef](#)]
28. Bunce, M.P.; Chinnathambi, P.; Blaxill, H.R. *The Effects of Pre-Chamber-Initiated Lean-Burn Combustion on Engine Efficiency and Emissions*; MAHLE Powertrain LLC: Plymouth, MI, USA, 2015.
29. *Control of Lean Mixtures*; SAE Technical Paper; SAE International: Warrendale, PA, USA, 1979.
30. Jamrozik, A. Lean combustion by a pre-chamber charge stratification in a stationary spark ignited engine. *J. Mech. Sci. Technol.* **2015**, *29*, 2269–2278. [[CrossRef](#)]
31. Liu, F.; Zhou, L.; Hua, J.; Liu, C.; Wei, H. Effects of pre-chamber jet ignition on knock and combustion characteristics in a spark ignition engine fueled with kerosene. *Fuel* **2021**, *293*, 120278. [[CrossRef](#)]
32. Novella, R.; Gómez-Soriano, J.; Martínez-Hernandiz, P.J.; Libert, C.; Rampanarivo, F. Improving the performance of the passive pre-chamber ignition concept for spark-ignition engines fueled with natural gas. *Fuel* **2021**, *290*, 119971. [[CrossRef](#)]
33. Benajes, J.; Novella, R.; Gómez-Soriano, J.; Martínez-Hernandiz, P.J.; Libert, C.; Dabiri, M. Evaluation of the passive pre-chamber ignition concept for future high compression ratio turbocharged spark-ignition engines. *Appl. Energy* **2019**, *248*, 576–588. [[CrossRef](#)]
34. Garcia-Oliver, J.M.; Niki, Y.; Rajasegar, R.; Novella, R.; Gomez-Soriano, J.; Martinez-Hernandiz, P.J.; Li, Z.; Musculus, M.P.B. An experimental and one-dimensional modeling analysis of turbulent gas ejection in pre-chamber engines. *Fuel* **2021**, *299*, 120861. [[CrossRef](#)]

35. Validi, A.; Schock, H.; Jaber, F. Turbulent jet ignition assisted combustion in a rapid compression machine. *Combust. Flame* **2017**, *186*, 65–82. [[CrossRef](#)]
36. Ju, D.; Huang, Z.; Li, X.; Zhang, T.; Cai, W. Comparison of open chamber and pre-chamber ignition of methane/air mixtures in a large bore constant volume chamber: Effect of excess air ratio and pre-mixed pressure. *Appl. Energy* **2020**, *260*, 114319. [[CrossRef](#)]
37. Boretti, A.A. Modelling auto ignition of hydrogen in a jet ignition pre-chamber. *Int. J. Hydrog. Energy* **2010**, *35*, 3881–3890. [[CrossRef](#)]
38. Tanoue, K.; Kimura, T.; Jimoto, T.; Hashimoto, J.; Moriyoshi, Y. Study of prechamber combustion characteristics in a rapid compression and expansion machine. *Appl. Therm. Eng.* **2017**, *115*, 64–71. [[CrossRef](#)]
39. Biswas, S.; Tanvir, S.; Wang, H.; Qiao, L. On ignition mechanisms of premixed CH₄/air and H₂/air using a hot turbulent jet generated by pre-chamber combustion. *Appl. Therm. Eng.* **2016**, *106*, 925–937. [[CrossRef](#)]
40. Liu, Z.; Zhou, L.; Liu, B.; Zhao, W.; Wei, H. Effects of equivalence ratio and pilot fuel mass on ignition/extinction and pressure oscillation in a methane/diesel engine with pre-chamber. *Appl. Therm. Eng.* **2019**, *158*, 113777. [[CrossRef](#)]
41. da Costa, R.B.R.; Teixeira, A.F.; Rodrigues Filho, F.A.; Pujatti, F.J.P.; Coronado, C.J.R.; Hernández, J.J.; Lora, E.E.S. Development of a homogeneous charge pre-chamber torch ignition system for an SI engine fuelled with hydrous ethanol. *Appl. Therm. Eng.* **2019**, *152*, 261–274. [[CrossRef](#)]
42. Alvarez, C.E.C.; Couto, G.E.; Roso, V.R.; Thiriet, A.B.; Valle, R.M. A review of prechamber ignition systems as lean combustion technology for SI engines. *Appl. Therm. Eng.* **2018**, *128*, 107–120. [[CrossRef](#)]
43. Xu, G.; Kotzagianni, M.; Kyrtatos, P.; Wright, Y.M.; Boulouchos, K. Experimental and numerical investigations of the unscavenged prechamber combustion in a rapid compression and expansion machine under engine-like conditions. *Combust. Flame* **2019**, *204*, 68–84. [[CrossRef](#)]
44. Yousefi, A.; Birouk, M. Investigation of natural gas energy fraction and injection timing on the performance and emissions of a dual-fuel engine with pre-combustion chamber under low engine load. *Appl. Energy* **2017**, *189*, 492–505. [[CrossRef](#)]
45. Richards, K.J.; Senecal, P.K.; Pomraning, E. *CONVERGE 3.0*; Convergent Science: Madison, WI, USA, 2022.
46. Han, Z.; Reitz, R.D. Turbulence modeling of internal combustion engines using RNG κ - ϵ models. *Combust. Sci. Technol.* **1995**, *106*, 267–295. [[CrossRef](#)]
47. Amsden, A.A.; Findley, M. *KIVA-3V: A Block-Structured KIVA Program for Engines with Vertical or Canted Valves*; Lawrence Livermore National Lab.(LLNL): Livermore, CA, USA, 1997.
48. Nasrifar, K. Comparative study of eleven equations of state in predicting the thermodynamic properties of hydrogen. *Int. J. Hydrog. Energy* **2010**, *35*, 3802–3811. [[CrossRef](#)]
49. Park, J.-W.; Pei, Y.; Zhang, Y.; Zhang, A.; Som, S. Optimizing Hydrogen Kinetics for Zero-Carbon Emission Transport Technologies. In Proceedings of the International Petroleum Technology Conference, Riyadh, Saudi Arabia, 21–23 February 2022; OnePetro: Richardson, TX, USA, 2022.
50. Burke, M.P.; Chaos, M.; Ju, Y.; Dryer, F.L.; Klippenstein, S.J. Comprehensive H₂/O₂ kinetic model for high-pressure combustion. *Int. J. Chem. Kinet.* **2012**, *44*, 444–474. [[CrossRef](#)]
51. Bradley, D.; Lawes, M.; Liu, K.; Verhelst, S.; Woolley, R. Laminar burning velocities of lean hydrogen–air mixtures at pressures up to 1.0 MPa. *Combust. Flame* **2007**, *149*, 162–172. [[CrossRef](#)]
52. Silva, M.R.; Ben Houidi, M.; Hlaing, P.; Sanal, S.; Cenker, E.; AlRamadan, A.; Chang, J.; Turner, J.; Im, H. *The Effects of Piston Shape in a Narrow-Throat Pre-Chamber Engine*; SAE Technical Paper; SAE International: Warrendale, PA, USA, 2022.
53. Hlaing, P.; Silva, M.; Marquez, M.E.; Cenker, E.; Ben Houidi, M.; Im, H.G.; Turner, J.W.G.; Johansson, B. Estimates of the air-fuel ratio at the time of ignition in a pre-chamber using a narrow throat geometry. *Int. J. Engine Res.* **2021**. [[CrossRef](#)]
54. Silva, M.; Sanal, S.; Hlaing, P.; Cenker, E.; Johansson, B.; Im, H.G. *A Computational Investigation of Fuel Enrichment in the Pre-Chamber on the Ignition of the Main Chamber Charge*; In SAE Technical Paper Series; SAE International: Warrendale, PA, USA, 2021. [[CrossRef](#)]
55. Silva, M.; Sanal, S.; Hlaing, P.; Cenker, E.; Johansson, B.; Im, H.G. *Effects of Geometry on Passive Pre-Chamber Combustion Characteristics*; SAE Technical Paper; SAE International: Warrendale, PA, USA, 2020.
56. Sanal, S.; Silva, M.; Hlaing, P.; Cenker, E.; Johansson, B.; Im, H.G. *A Numerical Study on the Ignition of Lean CH₄/Air Mixture by a Pre-Chamber-Initiated Turbulent Jet*; SAE Technical Paper; SAE International: Warrendale, PA, USA, 2020.
57. Silva, M.; Liu, X.; Hlaing, P.; Sanal, S.; Cenker, E.; Chang, J.; Johansson, B.; Im, H.G. Computational assessment of effects of throat diameter on combustion and turbulence characteristics in a pre-chamber engine. *Appl. Therm. Eng.* **2022**, *212*, 118595. [[CrossRef](#)]
58. Aljabri, H.H.; Babayev, R.; Liu, X.; Badra, J.; Johansson, B.; Im, H.G. *Validation of Computational Models for Isobaric Combustion Engines*; SAE Technical Paper Series; SAE International: Warrendale, PA, USA, 2020. [[CrossRef](#)]
59. Aljabri, H.; Liu, X.; Allehaibi, M.; AlRamadan, A.S.; Badra, J.; Ben Houidi, M.; Johansson, B.; Im, H.G. *Computational Investigation of the Effects of Injection Strategy and Rail Pressure on Isobaric Combustion in an Optical Compression Ignition Engine*; SAE Technical Paper; SAE International: Warrendale, PA, USA, 2021.
60. Meininger, R.D.; Kweon, C.-B.M.; Szedlmayer, M.T.; Dang, K.Q.; Jackson, N.B.; Lindsey, C.A.; Gibson, J.A.; Armstrong, R.H. Knock criteria for aviation diesel engines. *Int. J. Engine Res.* **2017**, *18*, 752–762. [[CrossRef](#)]
61. Sahoo, S.; Srivastava, D.K. Effect of compression ratio on engine knock, performance, combustion and emission characteristics of a bi-fuel CNG engine. *Energy* **2021**, *233*, 121144. [[CrossRef](#)]
62. Sementa, P.; de Vargas Antolini, J.B.; Tornatore, C.; Catapano, F.; Vaglieco, B.M.; Sánchez, J.J.L. Exploring the potentials of lean-burn hydrogen SI engine compared to methane operation. *Int. J. Hydrog. Energy* **2022**, *47*, 25044–25056. [[CrossRef](#)]

-
63. Ge, H.; Lee, B.; Parameswaran, S.; Zhao, P. Combustion, knock and emissions of a port-fueled spark-ignition hydrogen engine: A CFD study. In Proceedings of the 12th U. S. National Combustion Meeting, Virtual, 14 May 2021.
 64. Hlaing, P.; Echeverri Marquez, M.; Singh, E.; Almatrafi, F.; Cenker, E.; Ben Houidi, M.; Johansson, B. *Effect of Pre-Chamber Enrichment on Lean Burn Pre-Chamber Spark Ignition Combustion Concept with a Narrow-Throat Geometry*; SAE Technical Papers; SAE International: Warrendale, PA, USA, 2020; pp. 1–21. [[CrossRef](#)]